Three-dimensional imaging using spectral encoding heterodyne interferometry

D. Yelin, S. H. Yun, and B. E. Bouma

Harvard Medical School and the Wellman Center for Photomedicine, Massachusetts General Hospital, 55 Fruit Street, BAR 703, Boston, Massachusetts 02114

G. J. Tearney

Harvard Medical School, Wellman Center for Photomedicine and the Pathology Service, Massachusetts General Hospital, 50 Blossom Street, BAR 703, Boston, Massachusetts 02114

Received February 11, 2005

We present a novel heterodyne approach for performing fast, three-dimensional spectrally encoded imaging. Volumetric data of a volunteer's finger and of coin surfaces were acquired at a rate of 5 volume sets per second with a depth resolution of 145 μm. © 2005 Optical Society of America

OCIS codes: 170.2150, 170.6900, 110.1650, 170.4580.

Three-dimensional (3D) endoscopy that provides clinicians with depth information can greatly aid a variety of minimally invasive procedures. Depth-resolved imaging with a large, 3D field of view is, however, challenging when one is utilizing small-diameter flexible imaging probes such as borescopes, laparoscopes, and endoscopes. Confocal imaging through a fiber bundle using a high-numerical-aperture lens[1] is one solution to this problem. The 3D field of view for these devices, however, is limited to less than a few millimeters due to the small clear aperture of the objective lens and the low f-number required for high-resolution optical sectioning. Other methods, such as stereo imaging[2] and structured illumination,[3] have been proposed. These methods all require additional hardware for the probe, increasing the size, cost, and complexity of these devices. Spectrally encoded endoscopy[4] (SEE) uses a broadband light source and a diffraction grating to spectrally encode reflectance across a transverse line within the sample. A two–dimensional (2D) image is formed by slowly scanning this spectrally encoded line. This method requires only a single optical fiber, thereby permitting imaging through a small-diameter, flexible probe. Compared with images obtained with fiber-bundle endoscopes, SEE images can have a larger number of resolvable points and are free from pixelation artifacts. When combined with interferometry, SEE has the additional capability of providing 3D images. In a recent paper,[5] depth-resolved imaging was demonstrated by incorporating the SEE probe in the sample arm of a Michelson interferometer. In this approach, 2D speckle fringe patterns are recorded by a CCD camera at multiple longitudinal locations of the reference mirror. Subsequently, the depth information is extracted by comparing the fringes obtained at consecutive reference mirror positions. One problem with this approach is that the reference mirror must be held stationary within an optical wavelength during a single image (or line) acquisition time to avoid the loss of fringe visibility.[6] Scanning the reference mirror with such high fidelity over multiple discrete depths is quite challenging at the high rates required for real-time volumetric imaging.

In this Letter we demonstrate high-speed 3D SEE based on a new heterodyne detection scheme. Using a continuously scanned optical delay line and a standard photodetector, we demonstrate a 3D SEE system capable of acquiring 3D images at 5 Hz with a depth resolution of 145 μm.

A schematic of the experimental setup is shown in Fig. 1a. A broad-bandwidth titanium:sapphire laser (Femtolasers Produktions Femtosource integral OCT, center wavelength 800 nm, 150 nm FWHM bandwidth) was coupled into the input port of a single-mode fiber-optic 50/50 Michelson interferometer. To simulate a miniature endoscopic imaging probe, we chose to use a compact lens–grating design in which the beam was first focused by a lens (f = 40 mm, beam diameter 0.5 mm) and then diffracted by a transmission grating (Holographix LLC, 1000 lines/mm) to form a spectrally encoded line (x axis) on the surface of the sample. A galvanometric optical scanner was used for slow (y) axis scanning.[4] These parameters resulted in a spatial transverse resolution of approximately 80 μm. The image comprised 80 transverse resolvable points; each transverse spot was illuminated with a bandwidth of 1.9 nm. The overall power on the sample was 4 mW. A double-pass rapidly scanning optical delay[7] (RSOD) was used to control the group delay of the reference arm light. The RSOD scanned over a range of 1.5 mm at a rate of 1000 scans/s. The interference signal as a function of time was recorded, demodulated, and displayed in real time by a computer.

To better understand the underlying principle governing broad-spectrum illumination for encoding both transverse and depth dimensions, consider a sample comprising three discrete scattering points in the x–z plane, as illustrated in Fig. 1b. As the RSOD

0146-9592/05/141794-3/$15.00

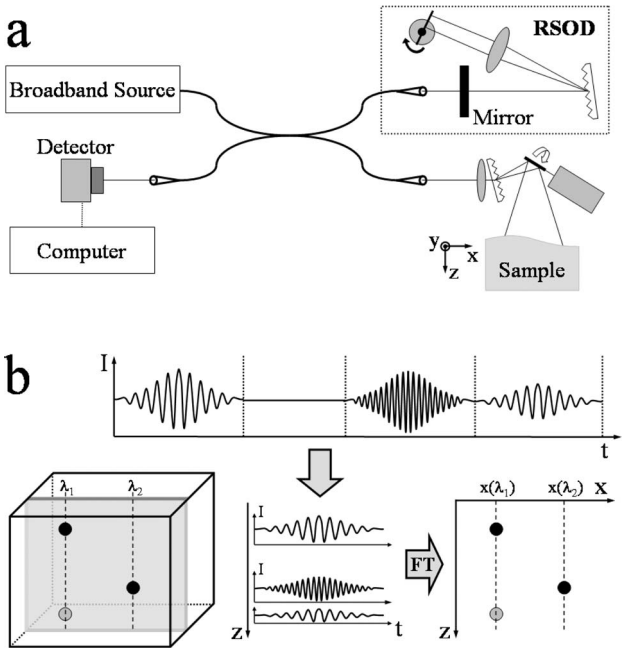

Fig. 1. a, Schematic of the time-domain spectrally encoded imaging system. b, Extraction of both transverse and depth information from the interference trace.

scans, the recorded signal as a function of time would contain three interference traces. Each interference trace represents depth information through its delay, $\Delta t_i = \Delta z_i / v_g$, where Δz_i is the depth location of the corresponding scatterer and v_g is the group-delay velocity, and transverse location through its carrier frequency, $2v_p/\lambda_i$, where v_p is the phase velocity and λ_i is the center wavelength at scatterer i ($i=1\ldots3$). The width of each trace determines the depth resolution and is given by $T_i = 0.44 N_x \lambda_i^2 / (v_g \Delta\lambda)$, where $\Delta\lambda$ is the total bandwidth and N_x is the number of resolvable points along the spectrally encoded line. A two-dimensional data set (x–z) can be obtained by applying a short-time Fourier transform (STFT) with a Gaussian window centered at Δt_i and with a width of T_i. The frequency distribution at a given Δt_i provides spatial information at the corresponding depth Δz_i. Alternatively, a depth-integrated transverse image can be obtained by Fourier transforming the entire raw data set at once or by summing individual depth-resolved images. Volumetric data are obtained by scanning the spectrally encoded line transversely across the sample.

Our detection scheme is analogous to that of conventional optical coherence tomography (OCT).[8] OCT uses broadband light to obtain relatively high axial resolution, <10 μm; however, to perform 3D imaging the probe beam needs to be scanned in two dimensions, requiring a fast beam-scanning mechanism. SEE uses the spectral bandwidth to obtain both transverse and axial resolution simultaneously, requiring only one slow-axis scan to acquire 3D data sets. For a given source bandwidth, this 2D resolution comes at the price of decreased axial resolution.

Assuming shot-noise-limited detection and a source with a uniformly flat spectrum, the signal-to-noise ratio (SNR) associated with a particular spatial point with reflectivity R is given by

$$\mathrm{SNR} = \frac{2\dfrac{P_r}{N_x} R \dfrac{P_s}{N_x}}{2h\nu P_r B} = \frac{2RP_s\tau}{h\nu N_x^2 N_z},$$

where P_r denotes the total reference arm power, P_s is the total sample power, τ is the line scan period, B is the sampling bandwidth, $B = N_z/2\tau$, and N_z corresponds to the number of axial resolvable points. Note that the SNR is inversely proportional to the square of the number of transverse resolvable points since only a fraction of the reference arm power (P_r/N_x) interferes with the light returning from a single transverse location.

Three-dimensional spectrally encoded imaging of a volunteer's finger is demonstrated in Fig. 2. The 3D data were captured at a rate of 2.5 frames/s; each frame consisted of 200 (spatially scanned axis) $\times$ 80 (wavelength encoded axis) $\times$ 10 (depth) points. The depth resolution was approximately 145 μm. A

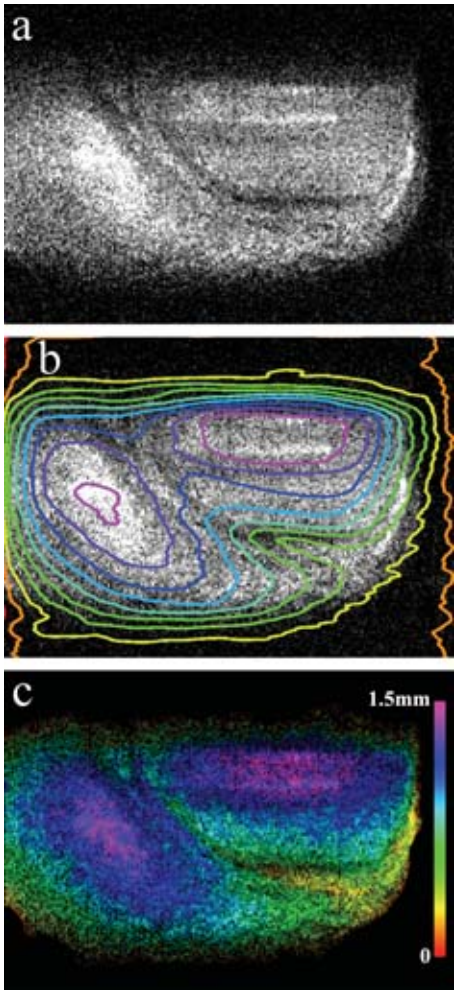

Fig. 2. 3D imaging of a volunteer's finger acquired in 0.4 s. a, 2D image of the finger (frame size 15 mm $\times$ 9 mm). Depth information is superimposed on the 2D image using b, contour lines and c, a false color height map.

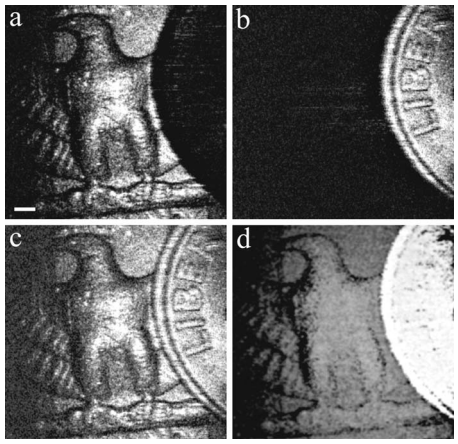

Fig. 3. Extended depth volumetric imaging of two coins. a, 2D image of the surface of a quarter (scale bar = 1 mm). b, 2D image of the surface of a dime placed 2.4 mm in front of the quarter, obtained after stepping the RSOD double-pass mirror by 2.4 mm. c, 2D depth-integrated view of the two coins. d, Depth-resolved image. The surface height is represented by a gray-scale lookup table, where depth locations closer to the lens have higher pixel intensity.

2D (depth-integrated) image is shown in Fig. 2a, obtained by acquiring and Fourier transforming 4000 points per scan. To extract the 3D information, each scan was divided into ten time windows that were transformed separately. The 3D data can be represented by a contour map and a false color image that are superimposed on the 2D image, as shown in Figs. 2b and 2c, respectively. In tissue, the single-scattered signal emerging from deep within the sample is considerably lower than that from the tissue surface. As a result, we have assumed that the largest frequency component of each STFT corresponds to surface height. Imaging a variety of human tissue samples in future work will test the validity of this assumption.

Three-dimensional imaging of samples with a depth range larger than the 1.5 mm provided by the RSOD can be accomplished by obtaining multiple volumetric data sets where each set is acquired with a different reference arm path length. To demonstrate this extended range acquisition, we imaged the surface of a dime placed 2.4 mm in front of a quarter. The $f = 40$ mm imaging lens was replaced with an $f = 65$ mm lens to provide a larger field of view and depth of focus. Two volumetric data sets were obtained by calculating the STFT for each of two locations of the RSOD double-pass mirror. The images comprised 200 horizontal lines, captured at a rate of 5 volume sets per second, and processed and displayed on the computer screen at a rate of 2.5 frames per second. A 2D, depth-sectioned image of the quarter is shown in Fig. 3a. Although the surfaces of both coins are within the focal depth of the lens, the dime was not seen in the image because of the limited scanning range of the RSOD. After adjusting the optical path length of the reference arm by stepping the RSOD double-pass mirror by 2.4 mm, the surface of the dime could be visualized (Fig. 3b). By combining the two volumetric data sets, we were able to obtain a depth-integrated 2D image (Fig. 3c) and an extended-range depth resolved image (Fig. 3d).

In summary, we have demonstrated a new technique capable of high-speed volumetric imaging within the confines of a miniature fiber-optic probe. Our time-domain 3D spectrally encoded imaging system provides high volume acquisition rates of up to 5 Hz with a depth resolution of 145 μm. Further improvements in spatial resolution (see the technical discussion in Ref. 4) and ranging depth are possible by using a broader bandwidth source[9] and an extended-range optical delay line.[10]

This study was funded by the Whitaker Foundation. D. Yelin's e-mail address is dyelin@partners.org.

References

1. Y. S. Sabharwal, A. R. Rouse, L. Donaldson, M. F. Hopkins, and A. F. Gmitro, Appl. Opt. **38**, 7133 (1999).
2. M. Chan, W. Lin, C. Zhou, and J. Y. Qu, Appl. Opt. **42**, 1888 (2003).
3. D. Karadaglic, T. Wilson, and R. Juskaitis, paper 4964-84 in *Photonics West 2003, Biomedical Optics* (SPIE CD-ROM).
4. G. J. Tearney, M. Shishkov, and B. E. Bouma, Opt. Lett. **27**, 412 (2002).
5. D. Yelin, B. E. Bouma, N. Iftimia, and G. J. Tearney, Opt. Lett. **28**, 2321 (2003).
6. S. H. Yun, G. J. Tearney, J. F. de Boer, and B. E. Bouma, Opt. Express **12**, 2977 (2004).
7. G. J. Tearney, B. E. Bouma, and J. G. Fujimoto, Opt. Lett. **22**, 1811 (1997).
8. D. Huang, E. A. Swanson, C. P. Lin, J. S. Schuman, W. G. Stinson, W. Chang, M. R. Hee, T. Flotte, K. Gregory, C. A. Puliafito, and J. G. Fujimoto, Science **254**, 1178 (1991).
9. A. Unterhuber, B. Povazay, K. Bizheva, B. Hermann, H. Sattmann, A. Stingl, T. Le, M. Seefeld, R. Menzel, M. Preusser, H. Budka, Ch. Schubert, H. Reitsamer, P. K. Ahnelt, J. E. Morgan, A. Cowey, and W. Drexler, Phys. Med. Biol. **49**, 1235 (2004).
10. K. K. M. B. D. Silva, A. V. Zvyagin, and D. D. Sampson, Electron. Lett. **35**, 1404 (1999).